IEEE Access
Multidisciplinary | Rapid Review | Open Access Journal

Received October 13, 2020, accepted October 19, 2020, date of publication October 29, 2020, date of current version November 12, 2020.

Digital Object Identifier 10.1109/ACCESS.2020.3034591

Geometric Optimization of Distributed MIMO Radar Systems With Spatial Distance Constraints

YAO WANG, (Graduate Student Member, IEEE), SHIXING YANG, (Graduate Student Member, IEEE), TAO ZHOU, (Member, IEEE), AND NA LI, (Member, IEEE)

School of Information and Communication Engineering, University of Electronic Science and Technology of China, Chengdu 611731, China

Corresponding author: Yao Wang (wangyaoee@std.uestc.edu.cn)

This work was supported in part by the National Natural Science Foundation of China under Grant 61701088, and in part by the Sichuan Science and Technology Project of China under Grant 2019JDRC0061.

ABSTRACT We consider a geometric optimization problem of distributed multi-input multi-output (MIMO) radar systems with widely separated radar nodes in this article. The aim is to maximize the radar surveillance performance in a given area of interest by adjusting the node positions, while satisfying practical spatial distance constraints among radar nodes. Typical constraints can be, for example, the maximum distance constraints between nodes and fusion centers (FCs) due to limited communication and the minimum distance constraints to ensure a better system spatial diversity. To achieve this goal, we first derive an analytical expression for a weighted coverage ratio (WCR) metric to evaluate the system surveillance performance. Then, using the WCR metric as the objective function, we formulate a spatial constrained geometric optimization problem for three typical MIMO radar system architectures, each of which has a unique expression of distance constraints. However, the formulated optimization problem is computationally intractable for practical scenarios due to its high dimensionality, non-convexity and especially the complex spatial constraints. To solve this problem, we propose an enhanced particle swarm optimization (PSO) algorithm, and different from the standard PSO, the particles of the proposed enhanced PSO can properly consider the distance constraints within themselves during swarm optimization process. Finally, various numerical studies show that the proposed method can effectively maximize the surveillance performance while satisfying the complex distance constraints.

INDEX TERMS Distributed MIMO radar, geometric optimization, distance constraints, radar surveillance performance, particle swarm optimization.

I. INTRODUCTION

Motivated by the recent advances in multiple-input multiple-output (MIMO) wireless communications [1], [2], MIMO radars continue to arouse the attention of the international radar community. Distributed MIMO radar systems comprise multiple, widely spaced transmitting and receiving radar nodes and transmit multiple orthogonal waveforms [3], [4]. Such radar systems can fully utilize spatial diversity by observing a target simultaneously from different aspect angles [3], [5], [6]. As shown in existing publications, due to the spatial diversity provided by the widely dispersed radar nodes [3], [4], [7], distributed MIMO radar systems offer a number of unique benefits including better detection performance [8], [9], more degrees of freedom [10], [11], higher spatial resolution [12], better spatial coverage [13], enhanced parameter identifiability [14], and higher localization accuracy [15], [16].

However, the performance of distributed MIMO radar systems, to a large extent, relies on the node positions. To fully utilize the spatial diversity, there have been various studies on optimizing the system performance by adjusting the node positions [16]–[22]. In general, researches on the optimization of the placement of radar nodes can be divided into two categories. The first group focuses on optimizing the system performance in a given position [16], [17], while the second group aims to optimize the performance in a specific area [18]–[22].

In [16], [17], different system performance in a given position is improved by adjusting the node positions. In [16],

The associate editor coordinating the review of this manuscript and approving it for publication was Mehmet Alper Uslu.

a convex optimization problem was formulated with respect to minimizing the Cramér-Rao lower bound (CRLB) for localization accuracy of one target, and it is shown that symmetric deployment of transmitting and receiving radar nodes around the target is optimal. Optimal antenna placement was analyzed in terms of minimizing the CRLB of velocity estimation error for a given target in [17]. Similar to [16], symmetrically placing the transmitting and receiving radar nodes was concluded as the best choice.

Nevertheless, the general application of distributed MIMO radar systems is to monitor a radar surveillance area (RSA), rather than to detect a target located at a given position. In addition, it is often necessary to refer to multi-target scenarios in terms of locating or tracking targets. Taking into account regional surveillance and multi-target situations, from practical perspective, we prefer to optimize node positions to improve the system performance in the entire RSA, rather than at the given position, as [18]–[22]. In [18], a radar node deployment problem aiming at improving the system detection performance in an entire surveillance area was studied, and a sequentially exhaustive enumeration method was proposed by discretizing the radar deployment area into multiple small grids. But it is computationally intractable in practical scenarios where a few radar nodes exist. To reduce the computation load, a node placement algorithm based on the particle swarm optimization (PSO) was proposed in [19], aiming to maximum the system surveillance performance, i.e., the detection performance in the entire RSA, with coverage ratio being the performance metric. In [20], an algorithm for the joint placement of transmitters and receivers in presence of multiple targets was proposed, considering both the system detection performance and localization performance. The system interference performance in multiple regions was considered in [21]. A multi-objective optimization problem with respect to the node positions was formulated, and solved by a solution based on multi-objective particle swarm optimization (MOPSO).

However, all the aforementioned works ignore the distance constraints that exist in distributed MIMO radar systems, and these constraints are important in practical applications [23]–[26]. The maximum distance constraint between receiving node and fusion center (FC) is an important issue to be addressed, considering the transmission of the received signal from receiving nodes to the FC. Specifically, for distributed MIMO radar systems, the signal received at the receiving nodes needs to be transmitted to the FC for jointly processing, normally via wireless data links or optical fibers. For both the transmission mediums, the farther transmission distances normally result in the higher transmission costs. Moreover, when applying wireless data links to long-distance signal transmission, it is also necessary to consider the signal propagation interruption affected by the earth curvature. Furthermore, if the transmission distance is too far, the system synchronization will be difficult to achieve and the data transmission capacity will be deteriorated.

Meanwhile, ignoring the minimum distance constraint among radar nodes can also cause a series of problems. For instance, a closer node distance results in mutual interference of signals more easily, and leads to energy supply problems for some radar systems as well. Additionally, to fully utilize spatial diversity and enhance anti-jamming potential and robustness of radar systems, the distances among nodes also need to be kept wide enough.

Therefore, we have to fully consider the distance constrains among nodes and FCs when optimizing radar node placement. In fact, similar constraints also have to be addressed in path planning [28], [29], array optimization problem [30], etc.

In this article, we establish an optimization problem of radar node placement, and aim to enhance the system surveillance performance by optimizing the node positions while satisfying practical spatial distance constraints.

The main contributions of our paper are listed as follows:

1) *Novel surveillance performance metric for the distributed MIMO radar*: We analyze the radar detection performance, and derive an analytical expression for the detection probability for distributed MIMO radar systems. Considering different levels of importance of sub-areas in the RSA, by setting weights to sub-areas, a weighted coverage ratio (WCR) constructed by the detection probability is proposed as the surveillance performance metric.
2) *Radar node placement optimization problem with complex constraints*: We propose a node placement optimization problem with generalized distance constraints, and introduce three typical system architectures for centralized fusion, which differs from each other in the expression of the maximum distance constraint. Additionally, to each system architecture, the specific expression of the maximum distance constraint is formulated.
3) *Fast solution to the non-convex problem with complex constraints*: Our presented optimization problem is high-dimensional, non-convex and nonlinear, and has complex constraints. Moreover, it differs from the structure of the optimization problem established in previous literature [16]–[21]. To solve such a problem efficiently, based on the standard PSO, we make improvements in the strategies of velocity update and the best position update of particles, and propose an internal self-constrained PSO (ISC-PSO) algorithm. In addition to driving the update of particles to directions for larger objective function values, the ISC-PSO algorithm also drives the update of particles to directions where more distance constraints could be satisfied.

Combining the proposed ISC-PSO algorithm and the established optimization condition according to the practical application scenario, we formulate a radar node placement algorithm. This algorithm satisfies all the distance constraints and meets requirements of the surveillance performance.

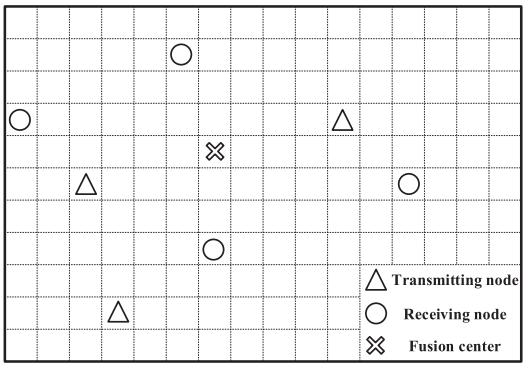

FIGURE 1. Sketch of the distributed MIMO radar system.

The rest of this article is organized as follows. The signal model is presented in section II. In section III, we formulate the optimal radar node placement problem. The WCR metric and the specific distance constraints for three system architectures are introduced. We propose a radar node placement algorithm to solve the formulated optimization problem in section IV. Section V presents simulation results and Section VI summarizes our contributions.

II. SYSTEM AND SIGNAL MODEL

We consider a widely distributed MIMO radar system equipped with M transmitting nodes and N receiving nodes, and thus there are $M \times N$ transmit-receive (T-R) channels. Denote $\mathbb{D} \subset \mathbb{R}^{2\times 1}$ the radar deployment area (RDA), where $\mathbb{R}$ is the real space. Let $\boldsymbol{\theta}_m^{\mathrm{t}} = [x_m^{\mathrm{t}}, y_m^{\mathrm{t}}]^{\mathsf{T}} \in \mathbb{D}$ and $\boldsymbol{\theta}_n^{\mathrm{r}} = [x_n^{\mathrm{r}}, y_n^{\mathrm{r}}]^{\mathsf{T}} \in \mathbb{D}$ denote the 2D Cartesian position coordinates of the mth transmitter and the nth receiver, respectively, where $m = 1, \ldots, M$ and $n = 1, \ldots, N$, and $(\cdot)^{\mathsf{T}}$ is the transpose operator. Let R_m^{t} denote the distance between the mth transmitter and the target and R_n^{r} denote the distance between the nth receiver and the target, and then

$$R_m^{\mathrm{t}} = \sqrt{(x_m^{\mathrm{t}} - x)^2 + (y_m^{\mathrm{t}} - y)^2}, \tag{1}$$

$$R_n^{\mathrm{r}} = \sqrt{(x_n^{\mathrm{r}} - x)^2 + (y_n^{\mathrm{r}} - y)^2}, \tag{2}$$

where $[x, y]^{\mathsf{T}}$ is the initial position coordinates of the target.

The transmitters use orthogonal waveforms to probe a common area of interest, and each receiver transmits the obtained orthogonal baseband signal to the FC for jointly processing. Then the FC collects the outputs from all receivers and returns a decision about the presence or absence of the target [4], [8]. The FC is selected from N receivers or is served by an external information processing center which is independent of the radar nodes, depending on the architecture of the radar system. In this article, three representative system architectures are considered, which will be introduced in detail later. The sketch of the considered distributed MIMO radar system is illustrated as Fig.1.

Consider one specific T-R channel consisting of the mth transmitter and the nth receiver. Let $s_m(t)$ denote K pulses sequentially transmitted by the mth transmitter at intervals of pulse repetition interval (PRI) during a coherent processing interval (CPI) [23], [31]–[33], [37]:

$$s_m(t) = \sum_{k=0}^{K-1} a_m(k) e^{j2\pi f_c(t-kT)} p(t - kT), \tag{3}$$

where $a_m(k)$ represents the amplitude of the kth pulse of $s_m(t)$ and $k = 0, \ldots, K-1$, $p(t)$ denotes the unit energy baseband equivalent of the transmitted pulse, T and f_c are respectively the PRI and the carrier frequency. We assume that the target moves towards the nth receiver with a radial velocity v_n, and the radar cross section (RCS) of the target follows the Swerling 0 model [31]. The received signal at the nth receiver at time t arising from signals transmitted by all transmitters and scattered by the target is expressed as [16], [31], [32], [34], [35]

$$\tilde{r}_n(t) \approx \sum_{m=1}^{M} s_m(t - \tau_{m,n}) l_{m,n}(k) e^{j\beta_{m,n}(k)} e^{j2\pi f_{d,n}(t-kT)}, \tag{4}$$

where $f_{d,n} = 2v_n f_c / c$ is the Doppler shift, and c represents the speed of light. Denote $\tau_{m,n}$ the time delay of the signal transmitted by the mth transmitter, scattered by the target, and received by the nth receiver, and $\tau_{m,n}$ is expressed as [34], [35]

$$\tau_{m,n} \approx \tau_{m,n}^0 - v_n t / c, \tag{5}$$

$$\tau_{m,n}^0 = (R_m^{\mathrm{t}} + R_n^{\mathrm{r}})/c. \tag{6}$$

The term $l_{m,n}(k) e^{j\beta_{m,n}(k)}$ in (4) is a complex parameter accounting for both propagation effects and scattering by the target [32], and the variation of $l_{m,n}(k)$ is given by [4], [16]

$$l_{m,n}(k) \propto 1/(R_m^{\mathrm{t}} R_n^{\mathrm{r}})^2. \tag{7}$$

During the K pulses within the CPI, we assume that the target does not move out the range bin. After down-modulating, the baseband equivalent signal at the nth receiver reduces to

$$r_n(t) \approx \sum_{m=1}^{M} \sum_{k=0}^{K-1} a_m(k) l_{m,n}(k) e^{j\beta_{m,n}(k)} e^{j2\pi f_{d,n}(t-kT)} \times p(t - kT - \tau_{m,n}^0). \tag{8}$$

Then the signals received at all the N receivers are sampled as data and transmitted to the FC to be processed jointly. Passing the data of all channels through a matched filter, the samples of the channel transmitted by the mth transmitter and received at the nth receiver can be obtained. In particular, if a target exists, and then a proper sample is selected according to the cell under test with respect to the kth pulse [23], [27]. In the signal-plus-noise hypothesis, the selected received sample from the kth pulse is given by [31], [36]

$$\begin{aligned} y_{m,n}(k) &= a_m(k) l_{m,n}(k) e^{j\beta_{m,n}(k)} e^{j2\pi f_{d,n} kT} + \xi_n(k), \\ &= A_{m,n}(k) e^{j\beta_{m,n}(k)} e^{j2\pi f_{d,n} kT} + \xi_n(k), \end{aligned} \tag{9}$$

where $A_{m,n}(k) = a_m(k) l_{m,n}(k)$ is the amplitude of the selected received sample, and $\xi_n(k)$ for $k = 0, \ldots, K-1$ are independent identically distributed (i.i.d) circular complex zero-mean Gaussian random variables.

Remark 1: The phases of the received signals for different channels are difficult to predict. Hence, data sampled for different channels are usually jointly processed by non-coherent processing instead of coherent processing [37], and as a result, the phase information is lost. Therefore we focus more on the amplitudes of the received samples.

Remark 2: From (1), (2), (7) and (9), we note that, for a given target, amplitudes of the received samples from all T-R channels are related to the positions of all radar nodes. Since the amplitudes affect the subsequent signal processing, with respect to different tasks (e.g. detection, surveillance, localization, velocity estimation, etc.), the performance of the distributed MIMO radar system significantly depends on the system spatial layout [3], [16], [17], [31], [38]. To improve the system performance, it is necessary to ensure the optimal or suboptimal node placement scheme.

III. PROBLEM FORMULATION

Long-term surveillance in a given area is one of the most common applications of radar systems. In this section, we derive a surveillance performance metric of the distributed MIMO radar system, and then the optimal radar node placement problem is established. Additionally, three representative system architectures of distributed MIMO radars adopting centralized fusion are presented.

A. THE OBJECTIVE FUNCTION OF THE SURVEILLANCE PERFORMANCE

The redeployment of radar nodes takes a certain amount of time. Hence the optimized system performance under consideration should be long-term effort. Herein, similar to [18], [19], [39], we focus on the system surveillance performance, and propose a WCR as the evaluation index. The calculation of the WCR is presented later.

In order to evaluate the system performance, the RDA and the RSA are both discretized into grids, and the system performance at any point within a grid is approximated by that at the center point of this grid. By the discretization of the area, the positions of all the grid points in the RSA form a matrix $\boldsymbol{\Psi}$:

$$\boldsymbol{\Psi} = [\boldsymbol{\psi}_1, \ldots, \boldsymbol{\psi}_q, \ldots, \boldsymbol{\psi}_Q], \tag{10}$$

where the position of the qth grid point in the RSA is denoted by $\boldsymbol{\psi}_q = [x_q^{\mathrm{g}}, y_q^{\mathrm{g}}]^{\mathsf{T}} \in \mathbb{R}^{2\times 1}$, $q = 1, \ldots, Q$, and Q denotes the total number of grids in the RSA.

The surveillance performance of the radar system depends on the system detection performance at all grid points of the RSA. Therefore, the system detection performance metric, which is dependent on the detection probability of the target and the probability of false alarm, needs to be derived first.

Consider the calculation of the detection probability of the target located at $[x, y]^{\mathsf{T}} = \boldsymbol{\psi}_q$. The K pulses from each T-R channel are first coherently processed, and then the detection problem can be formulated in terms of the following binary hypothesis test with respect to the T-R channel consisting of the mth transmitter and the nth receiver:

$$\begin{cases} H_1 : y_{m,n} = \sum_{k=0}^{K-1} A_{m,n}(k) e^{j\beta_{m,n}(k)} e^{j2\pi f_{d,n} kT} + \omega_n, \\ H_0 : y_{m,n} = \omega_n, \\ \qquad m = 1, \ldots, M, \ n = 1, \ldots, N, \end{cases} \tag{11}$$

where ω_n for $n = 1, \ldots, N$ are i.i.d complex zero-mean Gaussian random variables, and it is reasonable to assume that, for $n = 1, \ldots, N$, ω_n have the same variance σ^2 because the same receiving nodes are equipped in the radar system.

Then the data after coherent processing from different channels are incoherently processed, with the square-law detector applied. Let z be the test statistic given by [31]

$$z = \sum_{m=1}^{M} \sum_{n=1}^{N} |y_{m,n}|^2. \tag{12}$$

where $|\cdot|$ represents the modulus of a complex number. According to [31], [36], [38], [40], the probability of false alarm, P_{fa}, and the probability of detection of the target at $\boldsymbol{\psi}_q$, $P_d(\boldsymbol{\psi}_q)$, can be respectively calculated as below:

$$\begin{aligned} P_{fa} &= P\{z \geq \gamma | H_0\}, \\ &= \exp\left(-\frac{\gamma}{\sigma^2}\right) \sum_{i=0}^{M\times N-1} \frac{1}{i!} \left(\frac{\gamma}{\sigma^2}\right)^i, \end{aligned} \tag{13}$$

$$\begin{aligned} P_d(\boldsymbol{\psi}_q) &= P\{z \geq \gamma | H_1\}, \\ &= Q_{M\times N}\left(\sqrt{2 \sum_{m=1}^{M} \sum_{n=1}^{N} \sum_{k=1}^{K} \frac{A_{m,n}^2(k)}{\sigma^2}}, \sqrt{\frac{2\gamma}{\sigma^2}}\right), \\ &= Q_{M\times N}\left(\sqrt{2 \sum_{m=1}^{M} \sum_{n=1}^{N} \chi_{m,n,q}}, \sqrt{2\gamma / \sigma^2}\right), \end{aligned} \tag{14}$$

$$\chi_{m,n,q} = D_0 \frac{\sigma_{m,n} R_{\max}}{\sigma_0 (R_{m,q}^{\mathrm{t}} R_{n,q}^{\mathrm{r}})^2}, \tag{15}$$

where γ is the detection threshold, $Q_a(\cdot,\cdot)$ is the generalized Marcum Q-function of order a [31], $\chi_{m,n,q}$ denotes the signal-to-noise ratio (SNR) of the channel consisting of the mth transmitter and the nth receiver with respect to the given target at $\boldsymbol{\psi}_q$ after the coherent processing. Denote D_0 the detectability factor that satisfies the designed detection performance of the radar node, and $\sigma_{m,n}$, σ_0, $R_{\max}$, $R_{m,q}^{\mathrm{t}}$, $R_{n,q}^{\mathrm{r}}$ denote the bistatic RCS of the target, the monostatic RCS of the target, the maximum detectable distance of a single radar node (i.e., the distance between the radar node and the target when the output SNR is equal to D_0, with the monostatic radar of the same performance parameters adopted and K coherent processed pulses transmitted in a CPI), the distance between the position $\boldsymbol{\psi}_q$ and the mth transmitter, and the distance between $\boldsymbol{\psi}_q$ and the nth receiver, respectively.

According to (13), (14) and (15), we can calculate the probabilities of detection of the target considering all grids of the RSA where the target appears possibly. Then, focusing the system surveillance performance in the entire RSA, the WCR,

denoted by Γ, can be expressed as

$$\Gamma(\boldsymbol{\Theta}, \boldsymbol{\Psi}) = \mathbf{w}^{\mathsf{T}}\mathbf{c}(\boldsymbol{\Psi}) \times 100\% \tag{16}$$

where

$$\begin{aligned}
\mathbf{w} &= \left[w_1, \ldots, w_q, \ldots, w_Q\right]^{\mathsf{T}} \Big/ \sum_{q=1}^{Q} w_q \in \mathbb{R}^{Q\times 1}, \\
\mathbf{c}(\boldsymbol{\Psi}) &= [c_1(\boldsymbol{\psi}_1), \ldots, c_q(\boldsymbol{\psi}_q), \ldots, c_Q(\boldsymbol{\psi}_Q)]^{\mathsf{T}} \in \mathbb{R}^{Q\times 1}, \\
c_q(\boldsymbol{\psi}_q) &= \begin{cases} 1, & P_d(\boldsymbol{\psi}_q) \geq P_{dt}, \\ 0, & \text{others.} \end{cases}
\end{aligned} \tag{17}$$

In (16) and (17), $\boldsymbol{\Theta} = [\boldsymbol{\theta}_1^{\mathrm{t}}, \ldots, \boldsymbol{\theta}_M^{\mathrm{t}}, \boldsymbol{\theta}_1^{\mathrm{r}}, \ldots, \boldsymbol{\theta}_N^{\mathrm{r}}] \in \mathbb{R}^{2\times(M+N)}$ denotes the position matrix including all the radar nodes, $\mathbf{w}$ is a normalized weight value vector, whose element corresponds to a certain grid point and can be set according to the importance of the grid, and P_{dt} represents the required detection probability threshold.

Remark 3: Note that from (1), (2), (14), (15), (16) and (17), the WCR is related to the node positions and the location of the RSA. Once the RSA is determined, the WCR only depends on the node positions, and then $\Gamma(\boldsymbol{\Theta}, \boldsymbol{\Psi})$ *can be simplified as* $\Gamma(\boldsymbol{\Theta})$.

To ensure a satisfying surveillance performance of the radar system, it is necessary to optimize the node positions. As mentioned before, besides the surveillance performance, the localization performance and the velocity estimation performance, etc., are also related to the node positions [16], [17], but these are not the focus of this article.

B. PROBLEM FORMULATION

In this article, we consider enhancing the surveillance performance of the radar system via optimizing the node positions. To distributed MIMO radar systems, the establishment of the optimal node positions can be translated into an optimization problem as

$$\begin{aligned}
&\underset{\boldsymbol{\Theta}}{\text{maximize}} \quad \Gamma(\boldsymbol{\Theta}), \\
&s.t. \quad \boldsymbol{\theta}_m^{\mathrm{t}} \in \mathbb{D}, \ \boldsymbol{\theta}_n^{\mathrm{r}} \in \mathbb{D}, \\
&\qquad d_{\min} \leq d\left(\boldsymbol{\theta}_m^{\mathrm{t}}, \boldsymbol{\theta}_i^{\mathrm{t}}\right), \\
&\qquad d_{\min} \leq d\left(\boldsymbol{\theta}_n^{\mathrm{r}}, \boldsymbol{\theta}_j^{\mathrm{r}}\right), \\
&\qquad d\left(\boldsymbol{\theta}_n^{\mathrm{r}}, \boldsymbol{\theta}_{n,l}^{\mathrm{f}}\right) \leq d_{n\text{-max}}, \\
&\qquad m, i = 1, 2, \ldots, M, \ m \neq i, \\
&\qquad n, j = 1, 2, \ldots, N, \ n \neq j, \\
&\qquad l = 1, 2, \ldots, L,
\end{aligned} \tag{18}$$

where $\boldsymbol{\theta}_{n,l}^{\mathrm{f}} = [x_{n,l}^{\mathrm{f}}, y_{n,l}^{\mathrm{f}}]^{\mathsf{T}} \in \mathbb{D}$ denotes the position of the lth corresponding FC for the nth receiver (i.e., the lth FC connected with the nth receiver), and L is the number of the corresponding FCs for each receiver. Denote $d(\cdot,\cdot)$ the distance between any two radar nodes or between a node and an FC, $d_{\min}$ is the minimum distance constraint between radar nodes, and $d_{n\text{-max}}$ is the maximum distance constraint between the nth receiver and the corresponding FCs. Denote

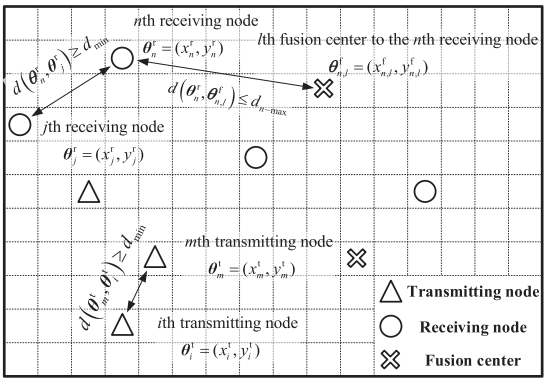

FIGURE 2. Sketch of the distributed MIMO radar system with the distance constraints.

$\boldsymbol{\Theta}_n^{\mathrm{f}} = \left[\boldsymbol{\theta}_{n,1}^{\mathrm{f}}, \ldots, \boldsymbol{\theta}_{n,L}^{\mathrm{f}}\right]$ the position matrix including all the corresponding FCs for the nth receiver, and the dimension of $\boldsymbol{\Theta}_n^{\mathrm{f}}$ depends on the architecture adopted by the radar system. The scene of the distributed MIMO radar system with the distance constraints is shown as Fig. 2.

We note that the constraints of the optimization problem (18) are mainly related to the limitations of signal transmission from receiving nodes to the FC, and are independent of the target detection. In other words, we cannot judge whether the constraints are satisfied only by the value of the objective function.

Remark 4: We note that the objective function and constraints of the optimization problem (18) are both related to the high-dimensional optimization variable $\boldsymbol{\Theta}$. *A randomly selected* $\boldsymbol{\Theta}$ *without being optimized can hardly satisfy the requirement for the surveillance performance or the distance constraints. Therefore, the optimization of node placement is an essential issue to be addressed to ensure better system performance and satisfy practical constraints.*

$$\begin{aligned}
&d\left(\boldsymbol{\theta}_n^{r}, \boldsymbol{\theta}_{n,l}^{f}\right) \leq d_{n\text{-max}}, \\
&\qquad n = 1, 2, \ldots, N, \quad l = 1, 2, \ldots, L.
\end{aligned} \tag{19}$$

In the optimization problem (18), (19) is the description of generalized maximum distance constraint. To different system architectures, the different methods of selecting FCs connected with the receiver lead to different specific expressions of (19). We will give detailed explanation below.

C. THE SPECIFIC EXPRESSIONS OF THE MAXIMUM DISTANCE CONSTRAINTS FOR DIFFERENT SYSTEM ARCHITECTURES

From the perspective of practical applications, we consider the distributed MIMO radar system adopting different system architectures for centralized fusion. Herein, three representative system architectures are studied [41], shown as Fig. 3.

1) CENTRAL NODE-TYPE ARCHITECTURE

To the central node-type architecture, simple receiving nodes are equipped to obtain the electromagnetic information of the target, but such receiving nodes do not have the ability

of information relay and information fusion processing. The radar system equips one or more external fixed FCs which are independent of the radar nodes, and each receiving node is connected to one certain FC. Such a system architecture is simple in structure and low in cost, but has poor robustness.

As we mentioned before, different maximum distance constraints would be established in the optimization problem considering different system architectures. To the central node-type architecture, the specific expression of (19) can be formulated as

$$\begin{cases} d\left(\boldsymbol{\theta}_n^{\mathrm{r}}, \boldsymbol{\theta}_{n,1}^{\mathrm{f}}\right) \le d_{n\text{-max}}, \\ n = 1, 2, \ldots, N. \end{cases} \tag{20}$$

2) NETTED ARCHITECTURE

To the netted architecture, complex receiving nodes are equipped, and such nodes have the ability of information relay and information fusion processing. In hostile environments, one of the receiving nodes is randomly selected as the FC. Due to the particularity of the FC selection, there has to be a communication link between any two receiving nodes. Such a system architecture is complex and costly with high robustness. After losing one or even more receiving nodes, the others can still integrate information and implement joint detection. To the netted architecture, the specific expression of (19) can be formulated as

$$\begin{cases} d\left(\boldsymbol{\theta}_n^{\mathrm{r}}, \boldsymbol{\theta}_j^{\mathrm{r}}\right) \le \min\left(d_{n\text{-max}}, d_{j\text{-max}}\right), \\ n, j = 1, 2, \ldots, N, n \ne j. \end{cases} \tag{21}$$

3) RINGED ARCHITECTURE

The ringed architecture is similar to the netted architecture, adopting the same receiving nodes and the same selection method of the FC. Different from the netted architecture, for the ringed architecture, only communication links between receiving nodes, which are with adjacent serial numbers or are corresponding to the minimum and the maximum serial numbers, are required. The ringed architecture is a compromised structure between the central node-type architecture and the netted architecture regarding robustness and cost. To the ringed architecture, the specific expression of (19) can be formulated as

$$\begin{cases} d\left(\boldsymbol{\theta}_k^{\mathrm{r}}, \boldsymbol{\theta}_{k+1}^{\mathrm{r}}\right) \le \min\left(d_{k\text{-max}}, d_{(k+1)\text{-max}}\right), \\ d\left(\boldsymbol{\theta}_N^{\mathrm{r}}, \boldsymbol{\theta}_1^{\mathrm{r}}\right) \le \min\left(d_{1\text{-max}}, d_{N\text{-max}}\right), \\ k = 1, \ldots, N-1. \end{cases} \tag{22}$$

So far, the optimization problem is introduced completely. The current problem is difficult to solve. First, it is a high-dimensional, non-convex, and nonlinear problem to jointly consider all node positions with no gradient information available. Second, consistent with the node positions, the proposed distance constraints are two-dimensional. In [30], a one-dimensional minimum distance constraint is considered in the sparse linear array design problem, and the optimization problem model is transformed to eliminate the constraint. However, this method has severe limitations and cannot be used to solve optimization problems with constraints above one dimension or with maximum distance constraints. Third, the maximum and the minimum distance constraints are coupled. In most cases, the two kinds of distance constraints are even contradictory, and this makes it intractable to simultaneously satisfy both kinds of constraints. Finally, intelligent optimization algorithms, such as the PSO algorithm and genetic algorithm, are generally used to solve such high-dimensional, non-convex, nonlinear optimization problems. However, these algorithms normally treat positions of all radar nodes as a whole to jointly optimize, without considering the system distance constraints. To reduce the computational burden and satisfy the distance constraints, we propose a novel and widely applicable node placement algorithm based on PSO in the next section.

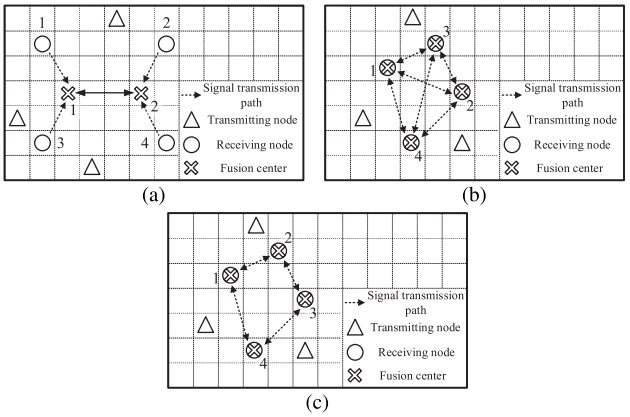

FIGURE 3. Sketch of three representative system architectures (The direction of the arrow represents the direction of signal transmission). (a). central node-type architecture; (b). netted architecture; (c). ringed architecture.

IV. NODE PLACEMENT ALGORITHM BASED ON PSO

The PSO algorithm is meta-heuristic in nature. It starts from a random solution, then searches the optimal solution through iterations with evaluating the qualities of solutions by an objective function [42], [43]. The PSO algorithm has been applied to many research fields, and it can greatly reduce the computational burden and allow us to get satisfying results [19], [21], [44]. However, the standard PSO algorithm is not suitable for solving optimization problems with complex constraints. Thus, based on the standard PSO, we propose a novel internal self-constrained PSO (ISC-PSO) algorithm to solve the proposed optimization problem with distance constraints. Next we describe the ISC-PSO algorithm.

Assuming that the swarm size is S (i.e., the number of particles is S), in the tth iteration, particle s, $s = 1, \ldots, S$ knows information about its current position, velocity, particle individual best position (its own best position it has visited so far) and the global best position of all particles (the best position all particles have visited so far), which are denoted by $X_s(t)$, $V_s(t)$, $\mathbf{Y}_s^{\mathrm{s}}(t)$ and $Y^{\mathrm{g}}(t)$, respectively. For optimization problem

of radar node placement, position of each particle represents a node placement scheme, and each column of the particle position is a coordinate of a certain node. Denote $\boldsymbol{x}^{\mathrm{t}}_{s,m}(t) \in \mathbb{D}$ and $\boldsymbol{x}^{\mathrm{r}}_{s,n}(t) \in \mathbb{D}$ the positions of the mth transmitter and the n receiver, where $m = 1, \ldots, M$ and $n = 1, \ldots, N$, then $X_s(t) = [\boldsymbol{x}^{\mathrm{t}}_{s,1}(t), \ldots, \boldsymbol{x}^{\mathrm{t}}_{s,M}(t), \boldsymbol{x}^{\mathrm{r}}_{s,1}(t), \ldots, \boldsymbol{x}^{\mathrm{r}}_{s,N}(t)]$. The position of the lth FC corresponding to the nth receiver is denoted by $\boldsymbol{x}^{\mathrm{f}}_{s,n,l}(t)$, where $l = 1, \ldots, L$.

To the particle s, initially, we randomly place all nodes in the RDA to get the initial particle position, and we initialize the particle velocity with a random velocity matrix. Then the position, velocity, individual best position of the particle and the global best position of all particles are updated in each iteration. In the process of initialization and iterations, the elements of particle positions are limited by the size of the RDA and the distance constraints, and the elements of particle velocities are limited by a fixed value $V_{\max}$, which is commonly determined by the size of the RDA.

A. THE IMPROVED RULE OF VELOCITY UPDATE OF PARTICLES

The standard PSO algorithm obtains information from the global best position and the individual best position of the particle s, respectively to establish the velocity components of particle s [21], [42], [43], as

$$V^{\mathrm{g}}_s(t+1) = c_1 r_1(t)(Y^{\mathrm{g}}(t) - X_s(t)), \tag{23}$$

$$V^{\mathrm{s}}_s(t+1) = c_2 r_2(t)(\mathbf{Y}^{\mathrm{s}}_s(t) - X_s(t)), \tag{24}$$

where c_k, $k = 1, 2$ are usually set as acceleration constants, $r_k(t)$, $k = 1, 2$ are independent random variables in the range of [0,1]. The particle velocity is then updated to push the particle position to directions where a better objective function value could be obtained.

However, such a rule of velocity update ignores the constraints within the particle. To consider the constraints, herein, in addition to the velocity update rule adopted by the standard PSO, we introduce the idea of virtual force [45], and propose a novel conditional velocity update method in the ISC-PSO algorithm. The proposed velocity update method provides the particle with velocity components conditionally, to compensate for the particle velocity when the the distance constraints are not satisfied, thereby prompting the satisfaction of the distance constraints among radar nodes and FCs.

Considering the mth transmitter, if the distance between the mth and the ith ($1 \le i \le M, i \ne m$) transmitters is less than $d_{\min}$, i.e., $d(\boldsymbol{x}^{\mathrm{t}}_{s,m}(t),\ \boldsymbol{x}^{\mathrm{t}}_{s,i}(t)) < d_{\min}$, a velocity component $\boldsymbol{v}^{\mathrm{t}}_{s,m,i\text{-min}} \in \mathbb{R}^{2\times 1}$ for the mth transmitter is established to increase the $d(\boldsymbol{x}^{\mathrm{t}}_{s,m}(t),\ \boldsymbol{x}^{\mathrm{t}}_{s,i}(t))$ and satisfy the minimum distance constraint. If $d(\boldsymbol{x}^{\mathrm{t}}_{s,m}(t),\ \boldsymbol{x}^{\mathrm{t}}_{s,i}(t)) \ge d_{\min}$, $\boldsymbol{v}^{\mathrm{t}}_{s,m,i\text{-min}}$ is assigned a two-dimensional zero vector, as (25). Different from $V^{\mathrm{g}}_s \in \mathbb{R}^{2\times(M+N)}$ and $V^{\mathrm{s}}_s \in \mathbb{R}^{2\times(M+N)}$, the proposed conditional components of particle velocity in ISC-PSO, are only corresponding to one certain radar node instead of all the nodes.

$$\boldsymbol{v}^{\mathrm{t}}_{s,m,i\text{-min}}(t+1) = \begin{cases} \mathbf{0}, \ \text{if } d(\boldsymbol{x}^{\mathrm{t}}_{s,m}(t),\ \boldsymbol{x}^{\mathrm{t}}_{s,i}(t)) \ge d_{\min}, \\ c_3 r_3(t)(\boldsymbol{x}^{\mathrm{t}}_{s,m}(t) - \boldsymbol{x}^{\mathrm{t}}_{s,i}(t)), \ \text{otherwise.} \end{cases} \tag{25}$$

A special case of $d(\boldsymbol{x}^{\mathrm{t}}_{s,m}(t),\ \boldsymbol{x}^{\mathrm{t}}_{s,i}(t)) < d_{\min}$ occurs when $d(\boldsymbol{x}^{\mathrm{t}}_{s,m}(t),\ \boldsymbol{x}^{\mathrm{t}}_{s,i}(t)) = 0$, i.e., the mth and the ith transmitters overlap, $\boldsymbol{v}^{\mathrm{t}}_{s,m,i\text{-ove}}$ is then established instead of $\boldsymbol{v}^{\mathrm{t}}_{s,m,i\text{-min}}$. If $d(\boldsymbol{x}^{\mathrm{t}}_{s,m}(t),\ \boldsymbol{x}^{\mathrm{t}}_{s,i}(t)) \ne 0$, $\boldsymbol{v}^{\mathrm{t}}_{s,m,i\text{-ove}}$ is assigned a two-dimensional zero vector, as

$$\boldsymbol{v}^{\mathrm{t}}_{s,m,i\text{-ove}}(t+1) = \begin{cases} \mathbf{0}, \ \text{if } d(\boldsymbol{x}^{\mathrm{t}}_{s,m}(t),\ \boldsymbol{x}^{\mathrm{t}}_{s,i}(t)) \ne 0, \\ c_4 r_4(t)\mathbf{e}, \ \text{otherwise,} \end{cases} \tag{26}$$

where $\mathbf{e}$ is a two-dimensional unit vector to an arbitrary direction, i.e., $\|\mathbf{e}\| = 1$ with $\|\cdot\|$ the Euclidean vector norm.

Similarly, considering the nth receiver, if the distance between the nth and the jth ($1 \le j \le N, j \ne n$) receivers is less than $d_{\min}$ or the two receivers overlap, i.e., $d(\boldsymbol{x}^{\mathrm{r}}_{s,n}(t),\ \boldsymbol{x}^{\mathrm{r}}_{s,j}(t)) < d_{\min}$ or $d(\boldsymbol{x}^{\mathrm{r}}_{s,n}(t),\ \boldsymbol{x}^{\mathrm{r}}_{s,j}(t)) = 0$, $\boldsymbol{v}^{\mathrm{r}}_{s,n,j\text{-min}}$ or $\boldsymbol{v}^{\mathrm{r}}_{s,n,j\text{-ove}}$ are established respectively. Otherwise, $\boldsymbol{v}^{\mathrm{r}}_{s,n,j\text{-min}}$ and $\boldsymbol{v}^{\mathrm{r}}_{s,n,j\text{-ove}}$ are assigned two-dimensional zero vectors, as (27) and (28),

$$\boldsymbol{v}^{\mathrm{r}}_{s,n,j\text{-min}}(t+1) = \begin{cases} 0, \ \text{if } d(\boldsymbol{x}^{\mathrm{r}}_{s,j}(t),\ \boldsymbol{x}^{\mathrm{r}}_{s,n}(t)) \ge d_{\min}, \\ c_3 r_3(t)(\boldsymbol{x}^{\mathrm{r}}_{s,n}(t) - \boldsymbol{x}^{\mathrm{r}}_{s,j}(t)), \ \text{otherwise,} \end{cases} \tag{27}$$

$$\boldsymbol{v}^{\mathrm{r}}_{s,n,j\text{-ove}}(t+1) = \begin{cases} \mathbf{0}, \ \text{if } d(\boldsymbol{x}^{\mathrm{r}}_{s,j}(t),\ \boldsymbol{x}^{\mathrm{r}}_{s,n}(t)) \ne 0, \\ c_4 r_4(t)\mathbf{e}, \quad \text{otherwise.} \end{cases} \tag{28}$$

Different from the transmitters, if the distance between the nth receiver and the lth corresponding FC is greater than $d_{n\text{-max}}$, i.e., $d(\boldsymbol{x}^{\mathrm{r}}_{s,n}(t), \boldsymbol{x}^{\mathrm{f}}_{s,n,l}(t)) > d_{n\text{-max}}$, a velocity component $\boldsymbol{v}^{\mathrm{r}}_{s,n,l\text{-max}}$ for the nth receiver is established to make the $d(\boldsymbol{x}^{\mathrm{r}}_{s,n}(t), \boldsymbol{x}^{\mathrm{f}}_{s,n,l}(t))$ decrease to satisfy the maximum distance constraint. If $d(\boldsymbol{x}^{\mathrm{r}}_{s,n}(t), \boldsymbol{x}^{\mathrm{f}}_{s,n,l}(t)) \le d_{n\text{-max}}$, $\boldsymbol{v}^{\mathrm{r}}_{s,n,l\text{-max}}$ is assigned a two-dimensional zero vector, as

$$\boldsymbol{v}^{\mathrm{r}}_{s,n,l\text{-max}}(t+1) = \begin{cases} \mathbf{0}, \ \text{if } d(\boldsymbol{x}^{\mathrm{r}}_{s,n}(t),\ X^{\mathrm{f}}_{s,n,l}(t)) \le d_{n\text{-max}}, \\ c_5 r_5(t)(\boldsymbol{x}^{\mathrm{f}}_{s,n,l}(t) - \boldsymbol{x}^{\mathrm{r}}_{s,n}(t)), \ \text{otherwise.} \end{cases} \tag{29}$$

Figs. 4(a), (b), and (c) show the directions of $\boldsymbol{v}^{\mathrm{r}}_{s,n,j\text{-min}}$, $\boldsymbol{v}^{\mathrm{r}}_{s,n,j\text{-ove}}$ and $\boldsymbol{v}^{\mathrm{r}}_{s,n,l\text{-max}}$, respectively. Similar to the standard PSO, in (25)-(29), $r_k(t)$, $k = 3, 4, 5$ are independent random variables in the range of [0,1], and c_k, $k = 3, 4, 5$ are set as constants which control the range of velocity compensation for particle elements, respectively corresponding to the three unsatisfied distance constraints. The values of c_k can be determined according to the specific optimization problem, mainly related to the types of unsatisfied distance constraints. For instance, c_3 corresponds to the unsatisfied minimum distance constraint. For this case, $d(\boldsymbol{x}^{\mathrm{r}}_{s,n}(t), \boldsymbol{x}^{\mathrm{r}}_{s,j}(t))$ is small. Recall (27), to obtain sufficient velocity compensation and then satisfy the minimum distance constraint, the value of c_3 should be relatively larger. In contrast, the value of c_5, which corresponds to the unsatisfied maximum distance constraint, should be relatively smaller. Meanwhile, the values of c_k are also related to the system architecture. For example,

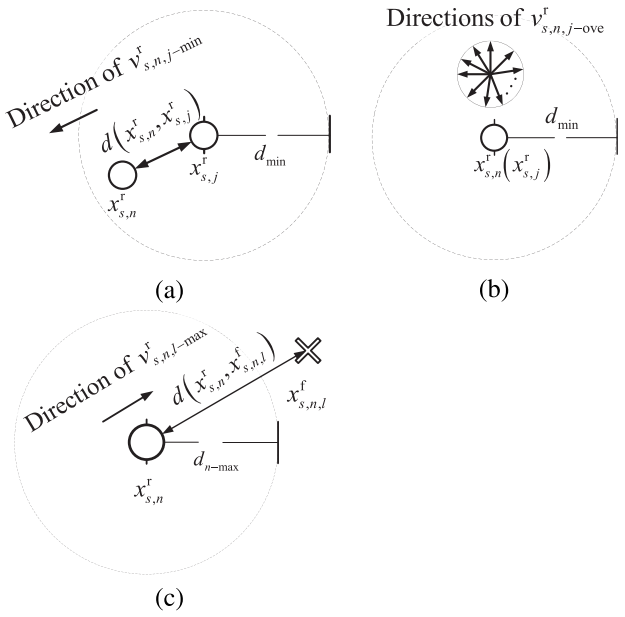

FIGURE 4. Sketch of directions of the proposed particle velocity components to satisfy the distance constraints. (a). $v^{r}_{s,n,j\text{-min}}$; (b). $v^{r}_{s,n,j\text{-ove}}$; (c). $v^{r}_{s,n,l\text{-max}}$.

when a netted architecture is adopted with all the distance constraints satisfied, the radar nodes get close because of the strong constraints. Thus, c_5 should be set small to provide subtle velocity compensation and prevent the algorithm being difficulty in convergence. In a sense, similar with the acceleration constants c_1 and c_2 used in the standard PSO, c_k herein are sort of empirical parameters [21], [42], [43], and how to choose the appropriate c_k to ensure fast and stable convergence of the algorithm deserves further research.

Considering the influence of all radar nodes comprehensively, for the mth transmitter, velocity components established for the cases corresponding to (25), (26) can be expressed as (30), (31), respectively,

$$\boldsymbol{v}^{t}_{s,m\text{-min}}(t+1) = \sum_{i=1,i\neq m}^{M} \boldsymbol{v}^{t}_{s,m,i\text{-min}}(t+1), \tag{30}$$

$$\boldsymbol{v}^{t}_{s,m\text{-}ove}(t+1) = \sum_{i=1,i\neq m}^{M} \boldsymbol{v}^{t}_{s,m,i\text{-}ove}(t+1). \tag{31}$$

For the nth receiver, besides the similar velocity components as established above for the cases corresponding to (27), (28), expressed as (32), (33), another velocity component corresponding to (29) is established as (34),

$$\boldsymbol{v}^{r}_{s,n\text{-min}}(t+1) = \sum_{j=1,j\neq n}^{N} \boldsymbol{v}^{r}_{s,n,j\text{-min}}(t+1), \tag{32}$$

$$\boldsymbol{v}^{r}_{s,n\text{-}ove}(t+1) = \sum_{j=1,j\neq n}^{N} \boldsymbol{v}^{r}_{s,n,j\text{-}ove}(t+1), \tag{33}$$

$$\boldsymbol{v}^{r}_{s,n\text{-max}}(t+1) = \sum_{l=1}^{L} \boldsymbol{v}^{r}_{s,n,l\text{-max}}(t+1). \tag{34}$$

Algorithm 1 Strategy of Velocity Update of Particles in ISC-PSO for Node Placement Optimization Problem

Initialize $\mathbf{V}_s(1)$;
for $t = 2, \ldots, T$ **do**
  for $s = 1, 2, \ldots, S$ **do**
    Calculate $V^{g}_{s}(t)$ and $V^{s}_{s}(t)$ according to (23) and (24);
    for $m = 1, 2, \ldots, M$ **do**
      Calculate $\boldsymbol{v}^{t}_{s,m\text{-min}}$ and $\boldsymbol{v}^{t}_{s,m\text{-}ove}$ according to (25), (26), (30) and (31), respectively;
    end for
    for $n = 1, 2, \ldots, N$ **do**
      Calculate $\boldsymbol{v}^{r}_{s,n\text{-min}}$, $\boldsymbol{v}^{r}_{s,n\text{-}ove}$ and $\boldsymbol{v}^{r}_{s,n\text{-max}}$ according to (27), (28), (29), (32), (33) and (34), respectively;
    end for
    Calculate the final $V_s(t)$ to update the position of the sth particle with the calculated $V^{g}_{s}(t)$, $V^{s}_{s}(t)$, $\boldsymbol{v}^{t}_{s,m\text{-min}}(t)$, $\boldsymbol{v}^{t}_{s,m\text{-}ove}(t)$, $\boldsymbol{v}^{r}_{s,n\text{-min}}(t)$, $\boldsymbol{v}^{r}_{s,n\text{-}ove}(t)$ and $\boldsymbol{v}^{r}_{s,n\text{-max}}(t)$.
  end for
end for

Now, we divide the integrated particle velocity update into two steps, formulated as:

The first stage:

$$\begin{aligned}\mathbf{V}_s(t+1,1) = \mu(t) \times \mathbf{V}_s(t,2) &+ c_1 r_1(t) \times (\mathbf{Y}^{g}(t) - \mathbf{X}_s(t)) \\ &+ c_2 r_2(t)(\mathbf{Y}^{s}_{s}(t) - \mathbf{X}_s(t)),\end{aligned} \tag{35}$$

and the second stage:

$$\begin{aligned}\boldsymbol{v}^{t}_{s,m}(t+1,2) &= \boldsymbol{v}^{t}_{s,m}(t+1,1) \\ &+ \sum_{i=1,i\neq m}^{M} c_3 r_3(t)(\boldsymbol{x}^{t}_{s,m}(t) - \boldsymbol{x}^{t}_{s,i}(t)) \\ &\times u(d_{min} - d(\boldsymbol{x}^{t}_{s,m}(t), \boldsymbol{x}^{t}_{s,i}(t))) \\ &+ \sum_{i=1,i\neq m}^{M} c_4 r_4(t)\delta(d(\boldsymbol{x}^{t}_{s,m}(t), \boldsymbol{x}^{t}_{s,i}(t))), \\ \boldsymbol{v}^{r}_{s,n}(t+1,2) &= \boldsymbol{v}^{r}_{s,n}(t+1,1) \\ &+ \sum_{j=1,j\neq n}^{N} c_3 r_3(t)(\boldsymbol{x}^{r}_{s,n}(t) - \boldsymbol{x}^{r}_{s,j}(t)) \\ &\times u(d_{min} - d(\boldsymbol{x}^{r}_{s,n}(t), \boldsymbol{x}^{r}_{s,j}(t))) \\ &+ \sum_{j=1,j\neq n}^{N} c_4 r_4(t)\delta(d(\boldsymbol{x}^{r}_{s,n}(t), \boldsymbol{x}^{r}_{s,j}(t))) \\ &+ \sum_{l=1}^{L} c_5 r_5(t)(\boldsymbol{x}^{f}_{s,n,l}(t) - \boldsymbol{x}^{r}_{s,n}(t)) \\ &\times u(d(\boldsymbol{x}^{r}_{s,n}(t), \boldsymbol{x}^{f}_{s,n,l}(t)) - d_{n\text{-max}}),\end{aligned} \tag{36, 37}$$

where $\mu(t)$ is the inertia weight which decreases with iterations, usually set as $\mu(t) = 0.9 - 0.5 \times (t/T)$ with T the

maximum iteration number of the algorithm [19], [43], and $\boldsymbol{v}_{s,m}^{\mathrm{t}}(t+1,g),\ g=1,2$ and $\boldsymbol{v}_{s,n}^{\mathrm{r}}(t+1,g),\ g=1,2$ denote the updated velocity components of particle s at the gth stage in the $(t+1)$th iteration, respectively corresponding to the mth transmitter and the nth receiver.

In (36), (37), we define the function u as:

$$u(x)=\begin{cases}1, & x>0,\\ 0, & x\le 0,\end{cases} \tag{38}$$

and the function δ as:

$$\delta(x)=\begin{cases}1, & x=0,\\ 0, & \text{others}.\end{cases} \tag{39}$$

After the particle velocity update, the position of the particle s is then updated as

$$\mathbf{X}_s(t+1)=\mathbf{X}_s(t)+\mathbf{V}_s(t+1,2). \tag{40}$$

Remark 5: It should be noted that, as we stated above, the velocity update process of the particle is divided into two stages. In the first stage, the information between particles is utilized, mainly to promote the evolution of the particle to directions where a better objective function value could be obtained. In the second stage, the velocity update process includes three parts, respectively corresponding to the three unsatisfied distance constraints. The information within the particle is utilized in this stage, mainly to promote the evolution of the particle to directions where more distance constraints could be satisfied.

B. THE IMPROVED STRATEGIES OF THE BEST POSITION UPDATE OF PARTICLES

In addition to the improvements of the particle velocity update, in the ISC-PSO algorithm, the best position update rules with respect to the individual and the global best positions, are also improved to drive the evolution of particles to directions where more distance constraints could be satisfied.

In contrast with the standard PSO algorithm, a constraint indicator function *count* is introduced in the ISC-PSO algorithm. To every node placement scheme, denoted by a particle position $X(t)$ (or $Y(t)$), the *count* $(X(t))$ (or *count* $(Y(t))$) is used to show the number of the node pairs that do not satisfy the distance constraints. In the process of the best position update, the constraint indicator function plays the role of selection and judgment.

The individual best position of particle s is updated as

$$\mathbf{Y}_s^{\mathrm{s}}(t)=\begin{cases}\mathbf{X}_s(t), & t=1,\\ \mathbf{X}_s(t), & t\ge 2,\{\Gamma(\mathbf{X}_s(t))>\Gamma(\mathbf{Y}_s^{\mathrm{s}}(t-1))\\ & \quad \&\&\ count(\mathbf{X}_s(t))=0\}\ \|\\ & \quad \left\{count(\mathbf{X}_s(t))<\min\left(count(\mathbf{Y}_s^{\mathrm{s}}(t'))\right)\right\},\\ & \quad t'=1,2,\ldots,t-1,\\ \mathbf{Y}_s^{\mathrm{s}}(t-1), & \text{others}.\end{cases} \tag{41}$$

where && and $\|$ are respectively the logical AND and OR operators. Similarly, the global best position of all particles is updated as

$$Y_{\text{g-select}}(t)=\arg\max_{Y_s^{\mathrm{s}}(t)}\Gamma(Y_s^{\mathrm{s}}(t)),\quad 1\le s\le S, \tag{42}$$

$$\mathbf{Y}^{\mathrm{g}}(t)=\begin{cases}\mathbf{Y}_{\text{g-select}}(t), & t=1,\\ \mathbf{Y}_{\text{g-select}}(t), & t\ge 2,\{count(\mathbf{Y}_{\text{g-select}}(t))=0\}\ \|\\ & \quad \left\{count(\mathbf{Y}_{\text{g-select}}(t))<\min\left(count(\mathbf{Y}^{\mathrm{g}}(t'))\right)\right\}\\ & \quad t'=1,2,\ldots,t-1,\\ \mathbf{Y}^{\mathrm{g}}(t-1), & \text{others}.\end{cases} \tag{43}$$

The best of the node placement schemes represented by all particles at the tth iteration is obtained as $Y^{\mathrm{g}}(t)$. The algorithm terminates after T iterations, and the final optimized node placement scheme is obtained as $Y^{\mathrm{g}}(T)$.

Algorithm 2 Node Placement Algorithm Based on ISC-PSO

for $s=1,2,\ldots,S$ **do**
  Initial $X_s(1)$ by giving each node a random position and $V_s(1)$ with limitation of a fix $V_{\max}$;
  Initial $Y_s^{\mathrm{s}}(1)$;
end for
Calculate $Y^{\mathrm{g}}(1)$;
for $t=2,\ldots,T$ **do**
  for $s=1,2,\ldots,S$ **do**
    Calculate $count(X_s(t-1))$, $count(Y_s^{\mathrm{s}}(t-1))$;
    Calculate $\Gamma(X_s(t-1))$, $\Gamma(Y_s^{\mathrm{s}}(t-1))$;
    Update the particle velocity and position, $V_s(t)$ and $X_s(t)$, according to (35), (36), (37) and (40), respectively;
    Update the particle individual best position, $Y_s^{\mathrm{s}}(t)$, according to (41);
  end for
  Calculate $count(Y^{\mathrm{g}}(t-1))$;
  Update the global best position of all particles, $Y^{\mathrm{g}}(t)$, according to (42) and (43).
end for
Output $Y^{\mathrm{g}}(T)$ as the final node placement scheme.

C. COMPLEXITY ANALYSIS

In this article, we analyze the computational complexity of the proposed ISC-PSO algorithm in terms of flops, with the standard PSO algorithm being the benchmark. We define one addition, subtraction, multiplication, division of two floating-point numbers, comparison operation and logical operation as a flop [46], and the computational complexities of vector operations is calculated considering the vector dimensions. Since we can get the result of the function u or δ through a comparison operation, we define one calculation of the function u or δ as a flop, too. Assume T_{P} and T_{I} are the iteration numbers when the PSO and the ISC-PSO respectively get convergence. Then the computational complexity analysis for both algorithms is given in TABLE 1 for comparison.

TABLE 1. Computational complexity analysis for the PSO and the ISC-PSO.

Step	Flops	
	PSO	ISC-PSO
Velocity and position update	$20T_{\mathrm{P}}S(M+N)$	$T_{\mathrm{I}}S\{20(M+N)$ $+4M(5M-4)$ $+2N(10N+6L-7)\}$
Individual best position update	$T_{\mathrm{P}}S$	$S(T_{\mathrm{I}}+8)(T_{\mathrm{I}}-1)/2$
Global best position update	$T_{\mathrm{P}}(S-1)$	$(T_{\mathrm{I}}+4)(T_{\mathrm{I}}-1)/2$ $+T_{\mathrm{I}}(S-1)$

In TABLE 1, computational complexities of all operations in each algorithm are given. We conclude that, by omitting the lower-order terms, the computational complexity of the standard PSO algorithm is $\mathcal{O}(T_{\mathrm{P}}S)$, while the computational complexity of the ISC-PSO algorithm is $\mathcal{O}\left(T_{\mathrm{I}}{}^{2}S\right)$. For the ISC-PSO algorithm, higher computational complexity is inevitable, because the processing of the complex distance constraints leads to a lot of calculation.

The proposed ISC-PSO algorithm will converge to a suboptimal feasible solution, to which all the distance constraints are satisfied. Several numerical simulations, which highlight the applicability and effectiveness of the ISC-PSO algorithm, are given in the next section.

Remark 6: It should be noted that, as mentioned before, the PSO algorithm has a wide range of application. The proposed ISC-PSO algorithm, which is based on the standard PSO, can also be widely applicable to various optimization problems with distance constraints, such as path planning, array optimization, etc.

V. NUMERICAL RESULTS

As stated above, in order to verify the applicability and effectiveness of the proposed ISC-PSO algorithm in different application scenarios, we consider:

- different algorithms, including the ISC-PSO with the standard PSO being the benchmark,
- different system architectures,
- different communication capabilities of receivers (i.e., different maximum distance constraints between different receivers and the corresponding FCs), and
- different numbers of FCs (for the central node-type architecture), and different radar node deployment scenarios (for the netted architecture).

For an intuitive analysis and meaningful conclusions, as a specific case of distributed MIMO radar systems with M transmitters and N receivers, radar systems with N_s dispersed nodes are studied in this section, and each node is equipped with a single antenna which can transmit and receive electromagnetic wave. The importance of all grid points in the RSA is assumed to be the same, i.e., all the elements of $\mathbf{w}$ have the same value, and then we use the coverage ratio as the objective function instead of the WCR.

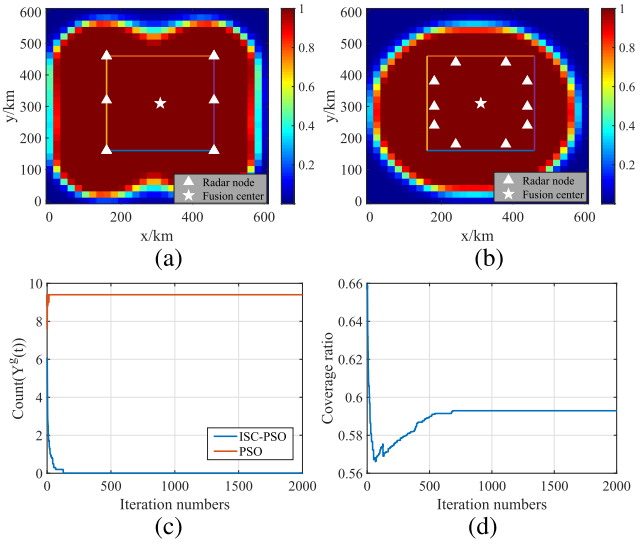

FIGURE 5. Optimization results of the central node-type architecture with a single FC (the values shown in the grids in (a), (b) represent the probabilities of detection [1]). (a). surveillance performance by the PSO; (b). surveillance performance by the ISC-PSO; (c). *count*$(Y^g(t))$; (d). coverage ratio by the ISC-PSO.

A. THE SAME COMMUNICATION CAPABILITIES OF RADAR NODES

We consider simulation scenarios where the communication capabilities of radar nodes are the same, i.e., the maximum distance constraints between the nodes and the corresponding FCs are the same. To three architectures, simulation scenarios are set as follows:

- the RSA is a square region of size 620 $km \times 620$ km,
- the RDA is a square region of size 300 $km \times 300$ km,
- the grid is also a square region of size 20 $km \times 20$ km, and
- the RDA is at the center of the RSA.

We use $N_s = 10$, $R_{\max} = 100$ km, $\sigma_{m,n} = \sigma_0 = 2$ m^2, $D_0 = 12.5$ dB, $P_{dt} = 0.8$, $P_{fa} = 10^{-6}$, $d_{\min} = 40$ km, and $d_{\max}$=150 km.

The standard PSO algorithm and the ISC-PSO algorithm are the same in some operations, and all the parameters used in the PSO, including c_1, c_2, S, T, $V_{\max}$, and the number of Monte Carlo runs, are also used in the ISC-PSO. Therefore, to compare the performance of both algorithms properly, in all simulations, the parameters mentioned above are set the same for both algorithms. For brevity, we just specify the parameters of the ISC-PSO and omit the repeated explanation of the parameters used by the PSO.

1) CENTRAL NODE-TYPE ARCHITECTURE

The parameters of ISC-PSO algorithm are as follows: c_1=c_2=2, c_3=3, c_4=5, c_5=0.8, S=400, T =2000, $V_{\max}$=12, and five Monte Carlo runs were performed.

[1]In the similar simulation results with respect to the surveillance performance below, the values shown in the grids also represent the probabilities of detection.

Fig. 5 shows the simulation results when the system adopts the central node-type architecture with one FC. From Fig. 5(c), we see that the iteration curve of the *count* ($Y^{g}(t)$) by the ISC-PSO decreases to zero at around 130 iterations. This shows that the initial random node placement scheme cannot satisfy all distance constraints, while the optimization process of the ISC-PSO lead to the satisfactory of more distance constraints, and all distance constraints get satisfied after about 130 iterations. In contrast, the iteration curve of the *count* ($Y^{g}(t)$) by the PSO remains at about 10 until the end of the iteration. This indicates that about 10 node pairs in the placement scheme obtained by the PSO do not satisfy the distance constraints. From Fig. 5(d), we see that the system surveillance performance has gone through two stages. In the first stage, the performance normally decreases to push more node pairs to satisfy the distance constraints. When the *count*($Y^{g}(t)$) decreases to zero, i.e., all node pairs satisfy the distance constraints, the second stage begins. In the second stage, the performance improves with iterations and all distance constraints are still satisfied. These two stages are corresponding in Figs. 5(c) and (d). Meanwhile, Figs. 5(c) and (d) show the results of satisfying the distance constraints and improving the system performance, respectively, which are the two goals that we focus on in this article.

In this simulation scenario, the FC is fixed at the center of the RDA and the positions of 10 nodes are optimized. However, in Fig. 5(a), there are only 6 nodes shown in the RDA because there are 4 nodes sharing overlapping positions with other nodes, and we can see that many node pairs do not satisfy the distance constraints as the result of the PSO algorithm. In contrast with the PSO, all node pairs can satisfy all the distance constraints when using the ISC-PSO algorithm, shown as Fig. 5(b). The above results prove that the system performance can be enhanced with the distance constraints satisfied by optimizing the node positions using the ISC-PSO algorithm.

We also observe that the placement scheme obtained by the ISC-PSO algorithm shows slightly weaker surveillance performance than that obtained by the PSO algorithm. This is reasonable due to the nature of the optimization problem, and this phenomenon is the result of compromise between surveillance mission and satisfaction of the distance constraints. When the maximum distance constraint exists, the nodes tend to be closer to the corresponding FCs, and this leads to the concentration of electromagnetic energy. As a result, the outer area cannot obtain enough electromagnetic energy to detect the target effectively.

Consider multiple fixed FCs for the central node-type architecture. We assume that the RDA is expanded to the same size as the RSA. When there are 2 FCs and 8 radar nodes, the nodes numbered 1, 2, 3, 4 are connected with the FC numbered 1, the nodes numbered 5, 6, 7, 8 are connected with the FC numbered 2. When there are 3 FCs and 9 radar nodes, the nodes numbered 1, 2, 3 are connected with the FC numbered 1, the nodes numbered 4, 5, 6 are connected with the FC numbered 2, and the nodes numbered 7, 8, 9 are connected with the FC numbered 3. The simulation results are shown as Fig. 6, and it is shown that we can still obtain a satisfying node placement scheme with the distance constraints satisfied using the proposed ISC-PSO algorithm.

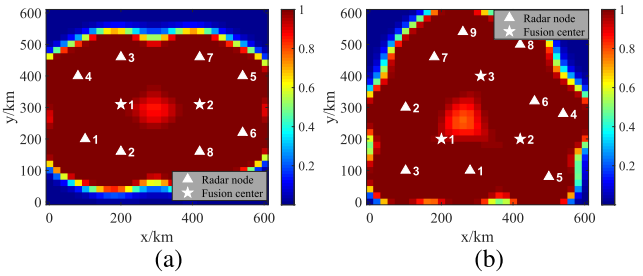

FIGURE 6. Optimized surveillance performance of the central node-type architecture with multiple FCs by the ISC-PSO. (a). two FCs; (b). three FCs.

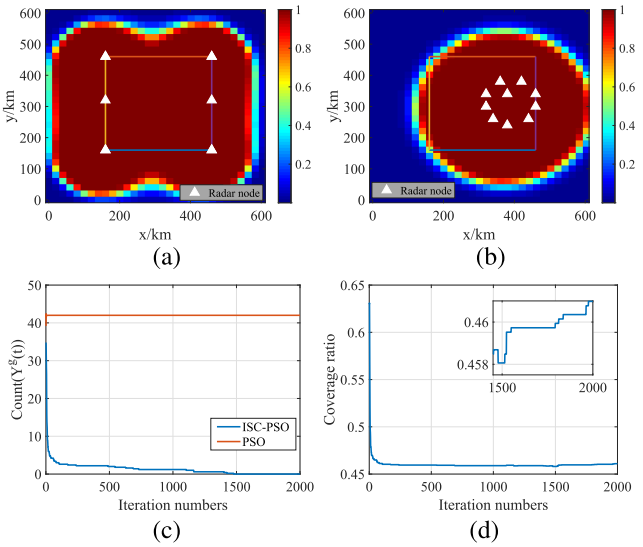

FIGURE 7. Optimization results of the netted architecture. (a). surveillance performance by the PSO; (b). surveillance performance by the ISC-PSO; (c). *count*($Y^{g}(t)$); (d). coverage ratio by the ISC-PSO.

2) NETTED AND RINGED ARCHITECTURES

The parameters of the ISC-PSO algorithm for both architectures are as follows: c_1=c_2=2, c_3=3, c_4=5, S=400, T = 2000, $V_{\max}$=12. We respectively chose c_5=0.1 and c_5=0.8 for the netted and the ringed architecture, and performed five Monte Carlo runs. Figs. 7 and 8 show the simulation results for the netted and the ringed architecture, respectively.

We observe that the results are nearly the same when the radar system adopts the netted architecture or the ringed architecture, as when the central node-type architecture is adopted. The results show that the system surveillance performance can be enhanced with the distance constraints satisfied by optimizing the node positions using the ISC-PSO algorithm, and the optimization process similarly undergoes through two stages. We also find that, when the netted architecture is adopted, in the second stage of the optimization process using the ISC-PSO algorithm, the increase of the

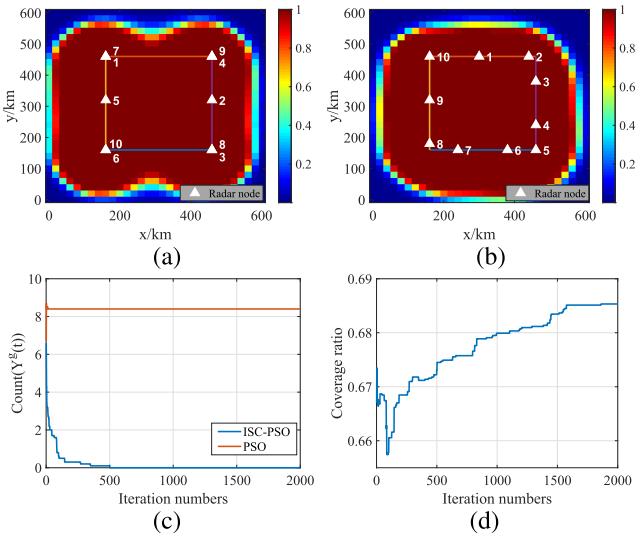

FIGURE 8. Optimization results of the ringed architecture. (a). surveillance performance by the PSO; (b). surveillance performance by the ISC-PSO; (c). *count*$(Y^g(t))$; (d). coverage ratio by the ISC-PSO.

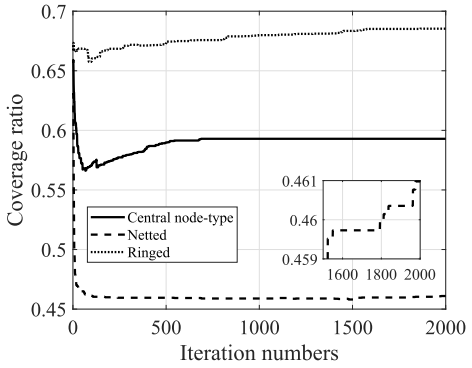

FIGURE 9. Comparison result of the surveillance performance of the radar systems adopting three architectures in the case of the same communication capabilities of radar nodes.

coverage ratio is inapparent, as shown in Fig. 7(d). This is due to the strict nature of the distance constraints with respect to the netted architecture. To satisfy such strict distance constraints, more nodes come close to each other, and this leads to the degradation of the system surveillance performance.

We also compare the optimized surveillance performance of the radar systems adopting three different architectures under the same simulation scenario and parameters, and the result is shown in Fig. 9. We observe that the radar system adopting the ringed architecture has the best surveillance performance, while the surveillance performance of the radar system adopting the netted architecture is the worst. Correspondingly, the radar system adopting the netted architecture is the most robust.

B. DIFFERENT COMMUNICATION CAPABILITIES OF RADAR NODES

We consider scenarios where the communication capabilities of radar nodes are different, i.e., the maximum distance

TABLE 2. Parameters of the ISC-PSO algorithm in the case of different communication capabilities of radar nodes with different system architectures.

Architectures parameters	Central node-type	Netted	Ringed
c_1	2	2	2
c_2	2	2	2
c_3	3	3	3
c_4	5	5	5
c_5	0.8	0.1	0.8
S	600	600	600
T	1200	1200	1200
$V_{\max}$	12	12	12

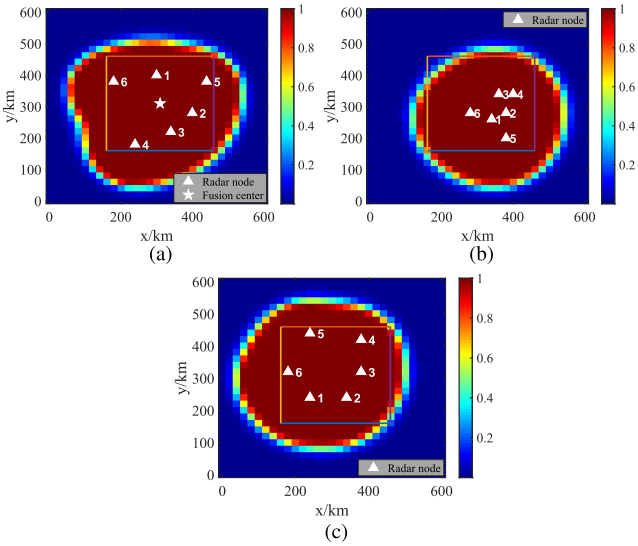

FIGURE 10. Optimization results of the surveillance performance in the case of different communication capabilities of radar nodes ($d_{\min}$ = 40 *km*, $d_{\max}$=[100, 100, 100, 150, 150, 150]$^{\mathrm{T}}$ *km*). (a). central node-type architecture; (b). netted architecture; (c). ringed architecture.

constraints between nodes and the corresponding FCs are different. Parameters for three architectures are set as follows:

- the RSA is a square region of size 620 $km \times 620$ km,
- the RDA is a square region of size 300 $km \times 300$ km,
- the grid is also a square region of size 20 $km \times 20$ km, and
- the RDA is at the center of the RSA.

We set $N_s = 6$, $R_{\max} = 100$ km, $\sigma_{m,n} = \sigma_0 = 2m^2$, $D_0 = 12.5$ dB, $P_{dt} = 0.8$, $P_{fa} = 10^{-6}$, and $d_{\min} = 40$ km. The maximum distance constraints between nodes and the corresponding FCs are expressed by $d_{\max}$, and $d_{\max}$=[100, 100, 100, 150, 150, 150]$^{\mathrm{T}}$ km (The order of the elements of $d_{\max}$ is consistent with the order of the radar nodes). The parameters of the ISC-PSO algorithm for three architectures are given in TABLE 2 and the simulation results are shown in Fig. 10. From Fig. 10, we see that the nodes spread as far as possible to obtain better surveillance performance with all the distance constraints still satisfied, although the maximum distance constraints between nodes and the corresponding FCs are different.

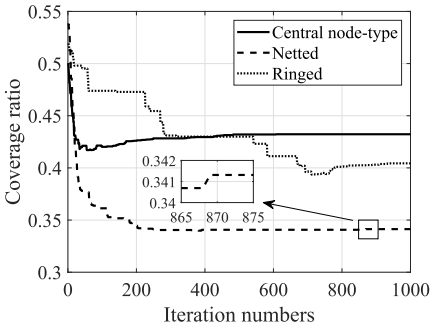

FIGURE 11. Comparison result of the surveillance performance of the radar systems adopting three architectures in the case of different communication capabilities of radar nodes.

As we did in the above case, in the case of different communication capabilities of radar nodes, we compare the optimized surveillance performance of the radar systems adopting three different architectures under the same simulation scenario and parameters. The result is shown as Fig. 11. We are surprised to find that, different from the case where the nodes have the same communication capabilities, when $d_{\max} = [100, 100, 100, 150, 150, 150]^{\mathsf{T}}$ km, the surveillance performance of the radar system adopting the netted architecture is still the worst. However, the system adopting the central node-type architecture has the best surveillance performance instead of that adopting the ringed architecture. Based on these results we conclude that, when the communication capabilities of the radar nodes change, the corresponding architecture that enables the system to achieve the optimal surveillance performance may also change. Therefore, the architecture selection of radar system is also an important issue to be considered, and deserves further investigation.

C. APPLICATION SCENARIOS

In this subsection, we consider two realistic and more challenging application scenarios where the RDA and the RSA are non-overlapping, shown as Fig. 12. Such scenarios commonly appears in the applications of area-denial and the defense of open sea. The radar systems for both the simulations below adopt the netted architecture which enforces the most strict distance constraints. The communication capabilities of radar nodes are assumed to be the same, and the parameters of the ISC-PSO algorithm is given in TABLE 3 with the repetitive parameters of the PSO omitted.

1) APPLICATION SCENARIO I

In this scenario, the boundary of the RDA and the RSA is smooth. The whole area is a square region of size 700 $km \times$ 480 km, the region where $0 \le y \le 200km$ is the RDA, and the region where $200km \le y \le 480km$ is the RSA. We set $d_{\min} = 40km$, $d_{\max} = 360km$, and $N_s = 10$. Simulation results for this case are shown in Fig. 13.

From Fig. 13, we observe that both node deployment schemes guarantee good surveillance performance by deploying radar nodes at the boundary of the RDA and the RSA. In such a situation, to satisfy the distance constraints, the relative positional relationship of the nodes is uniquely determined, and each node is kept 40 kilometers away from the nearest nodes. Hence the enforcement of the distance constraints is strict. Similar to the simulation results presented previously, we observe that some nodes overlap when using the PSO algorithm. In contrast, we can obtain an accurate node placement scheme using the ISC-PSO algorithm.

TABLE 3. Parameters of the ISC-PSO for both application scenarios.

Scenarios parameters	Scenarios I	Scenarios II
c_1	2	2
c_2	2	2
c_3	3	3
c_4	5	5
c_5	0.1	0.1
S	600	600
T	1200	1200
$V_{\max}$	12	12

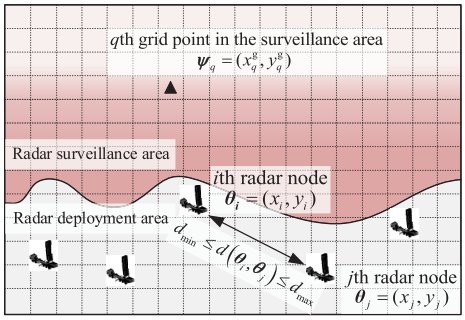

FIGURE 12. Sketch of the RDA and the RSA in application scenarios.

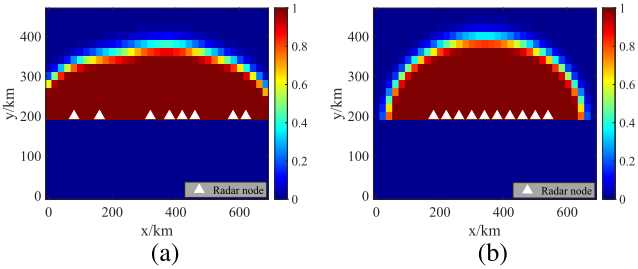

FIGURE 13. Optimization results. (a). surveillance performance by the PSO; (b). surveillance performance by the ISC-PSO.

2) APPLICATION SCENARIO II

In this scenario, the RDA has a convex surface facing the RSA. The whole area is a square region of size 400 $km \times$ 360 km, the region below the solid line is the RDA, and the region above the solid line is the RSA. We set $d_{\min} = 40km$, $d_{\max} = 150km$, and $N_s = 5$. Fig. 14 shows the corresponding simulation results.

From Fig.14(a), we see that all the optimized node positions obtained by the PSO algorithm gather in the protruding

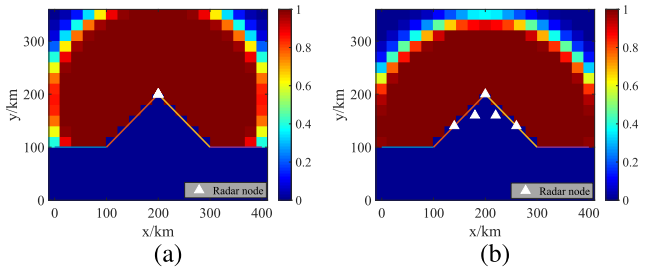

FIGURE 14. Optimization results. (a). surveillance performance by the PSO; (b). surveillance performance by the ISC-PSO.

position of the RDA and even overlap. The radar systems adopting such a deployment scheme is easy to be hit and destroyed, and the spatial diversity gain cannot be well utilized. Hence such a deployment scheme is not advisable. In contrast, the deployment scheme obtained by the ISC-PSO algorithm is satisfactory. From Fig.14(b), we observe that all the distance constraints are satisfied, and the optimized node positions are properly dispersed, to fully utilize the spatial diversity gain and get stronger robustness.

This set of simulations further illustrates the necessity of introducing distance constraints when optimizing the node positions, and verifies the applicability and effectiveness of the proposed ISC-PSO algorithm.

VI. CONCLUSION

We have studied an optimization problem of node placement with distance constraints in this article. We have derived an analytical expression for the detection probability for distributed MIMO radar systems, and have formulated a node placement optimization problem with distance constraints. Then a node placement algorithm based on the ISC-PSO has been proposed to solve the formulated optimization problem with complex constraints. Our simulation results have demonstrated the effectiveness of the proposed node placement algorithm.

REFERENCES

[1] S. M. Alamouti, "A simple transmit diversity technique for wireless communications," *IEEE J. Sel. Areas Commun.*, vol. 16, no. 8, pp. 1451–1458, Oct. 1998.

[2] G. J. Foschini, "Layered space-time architecture for wireless communication in a fading environment when using multi-element antennas," *Bell Labs Tech. J.*, vol. 1, no. 2, pp. 41–59, Aug. 2002.

[3] E. Fishler, A. Haimovich, R. S. Blum, L. J. Cimini, D. Chizhik, and R. A. Valenzuela, "Spatial diversity in radars-Models and detection performance," *IEEE Trans. Signal Process.*, vol. 54, no. 3, pp. 823–838, Mar. 2006.

[4] A. Haimovich, R. Blum, and L. Cimini, "MIMO radar with widely separated antennas," *IEEE Signal Process. Mag.*, vol. 25, no. 1, pp. 116–129, Jan. 2008.

[5] E. Fishler, A. Haimovich, R. Blum, D. Chizhik, L. Cimini, and R. Valenzuela, "MIMO radar: An idea whose time has come," in *Proc. IEEE Radar Conf.*, Philadelphia, PA, USA, Apr. 2004, pp. 71–78.

[6] E. Fishler, A. Haimovich, R. Blum, R. Cimini, D. Chizhik, and R. Valenzuela, "Performance of MIMO radar systems: Advantages of angular diversity," in *Proc. 38th Asilomar Conf. Signals Syst. Comput.*, Pacific Grove, CA, USA, Nov. 2004, pp. 305–309.

[7] H. Griffiths, "Multistatic, MIMO and networked radar: The future of radar sensors?" in *Proc. 7th Eur. Radar Conf.*, Paris, France, Sep./Oct. 2010, pp. 81–84.

[8] Q. He, N. H. Lehmann, R. S. Blum, and A. M. Haimovich, "MIMO radar moving target detection in homogeneous clutter," *IEEE Trans. Aerosp. Electron. Syst.*, vol. 46, no. 3, pp. 1290–1301, Jul. 2010.

[9] B. Shtarkalev and B. Mulgrew, "Multistatic moving target detection in unknown coloured Gaussian interference," *Signal Process.*, vol. 115, pp. 130–143, Oct. 2015.

[10] D. W. Bliss and K. W. Forsythe, "Multiple-input multiple-output (MIMO) radar and imaging: Degrees of freedom and resolution," in *Proc. IEEE Conf. Rec. 37th Asilomar Conf. Signals Syst. Comput.*, Pacific Grove, CA, USA, Nov. 2003, pp. 54–59.

[11] W. Yi, Y. Yuan, R. Hoseinnezhad, and L. Kong, "Resource scheduling for distributed multi-target tracking in netted colocated MIMO radar systems," *IEEE Trans. Signal Process.*, vol. 68, pp. 1602–1617, Feb. 2020.

[12] F. C. Robey, S. Coutts, D. Weikle, J. C. McHarg, and K. Cuomo, "MIMO radar theory and experimental results," in *Proc. 38th Asilomar Conf. Signals Syst. Comput.*, Pacific Grove, CA, USA, Nov. 2004, pp. 300–304.

[13] D. R. Fuhrmann and G. San Antonio, "Transmit beamforming for MIMO radar systems using signal cross-correlation," *IEEE Trans. Aerosp. Electron. Syst.*, vol. 44, no. 1, pp. 171–186, Jan. 2008.

[14] J. Li, P. Stoica, L. Xu, and W. Roberts, "On parameter identifiability of MIMO radar," *IEEE Signal Process. Lett.*, vol. 14, no. 12, pp. 968–971, Dec. 2007.

[15] W. Yi, T. Zhou, Y. Ai, and R. S. Blum, "Suboptimal low complexity joint multi-target detection and localization for non-coherent MIMO radar with widely separated antennas," *IEEE Trans. Signal Process.*, vol. 68, pp. 901–916, Jan. 2020.

[16] H. Godrich, A. M. Haimovich, and R. S. Blum, "Target localization accuracy gain in MIMO radar-based systems," *IEEE Trans. Inf. Theory*, vol. 56, no. 6, pp. 2783–2803, Jun. 2010.

[17] Q. He, R. S. Blum, H. Godrich, and A. M. Haimovich, "Target velocity estimation and antenna placement for MIMO radar with widely separated antennas," *IEEE J. Sel. Topics Signal Process.*, vol. 4, no. 1, pp. 79–100, Feb. 2010.

[18] M. Radmard, M. M. Chitgarha, M. N. Majd, and M. M. Nayebi, "Antenna placement and power allocation optimization in MIMO detection," *IEEE Trans. Aerosp. Electron. Syst.*, vol. 50, no. 2, pp. 1468–1478, Apr. 2014.

[19] Y. Yang, W. Yi, T. Zhang, G. Cui, L. Kong, X. Yang, and J. Yang, "Fast optimal antenna placement for distributed MIMO radar with surveillance performance," *IEEE Signal Process. Lett.*, vol. 22, no. 11, pp. 1955–1959, Nov. 2015.

[20] J. Yi, X. Wan, H. Leung, and M. Lü, "Joint placement of transmitters and receivers for distributed MIMO radars," *IEEE Trans. Aerosp. Electron. Syst.*, vol. 53, no. 1, pp. 122–134, Feb. 2017.

[21] T. Zhang, J. Liang, Y. Yang, G. Cui, L. Kong, and X. Yang, "Antenna deployment method for multistatic radar under the situation of multiple regions for interference," *Signal Process.*, vol. 143, pp. 292–297, Feb. 2018.

[22] C. Niu, Y. Zhang, and J. Guo, "Pareto optimal layout of multistatic radar," *Signal Process.*, vol. 142, pp. 152–156, Jan. 2018.

[23] M. A. Richards, J. A. Scheer, and W. A. Holm, *Principles of Modern Radar: Basic Principles*. New York, NY, USA: SciTech, 2010, pp. 547–587.

[24] B. Paul, A. R. Chiriyath, and D. W. Bliss, "Survey of RF communications and sensing convergence research," *IEEE Access*, vol. 5, pp. 252–270, Feb. 2017.

[25] F. Liu, C. Masouros, A. Li, H. Sun, and L. Hanzo, "MU-MIMO communications with MIMO radar: From co-existence to joint transmission," *IEEE Trans. Wireless Commun.*, vol. 17, no. 4, pp. 2755–2770, Apr. 2018.

[26] M. I. Skolnik, *Radar Handbook*, 3rd ed. New York, NY, USA: McGraw-Hill, 2008, pp. 1148–1153.

[27] M. A. Richards, *Fundamentals of Radar Signal Processing*. New York, NY, USA: McGraw-Hill, 2005, pp. 440–536.

[28] Y. Wang, T. Kirubarajan, R. Tharmarasa, R. Jassemi-Zargani, and N. Kashyap, "Multiperiod coverage path planning and scheduling for airborne surveillance," *IEEE Trans. Aerosp. Electron. Syst.*, vol. 54, no. 5, pp. 2257–2273, Oct. 2018.

[29] W. Shi, J. Li, W. Xu, H. Zhou, N. Zhang, S. Zhang, and X. Shen, "Multiple drone-cell deployment analyses and optimization in drone assisted radio access networks," *IEEE Access*, vol. 6, pp. 12518–12529, Feb. 2018.

[30] X. Yu, G. Cui, S. Yang, L. Kong, and W. Yi, "Coherent unambiguous transmit for sparse linear array with geography constraint," *IET Radar, Sonar Navigat.*, vol. 11, no. 2, pp. 386–393, Feb. 2017.
[31] G. Cui, A. DeMaio, and M. Piezzo, "Performance prediction of the incoherent radar detector for correlated generalized swerling-chi fluctuating targets," *IEEE Trans. Aerosp. Electron. Syst.*, vol. 49, no. 1, pp. 356–368, Jan. 2013.
[32] E. Conte and G. Ricci, "Performance prediction in compound-Gaussian clutter," *IEEE Trans. Aerosp. Electron. Syst.*, vol. 30, no. 2, pp. 611–616, Apr. 1994.
[33] J. Li and R. Wu, "An efficient algorithm for time delay estimation," *IEEE Trans. Signal Process.*, vol. 46, no. 8, pp. 2231–2235, Aug. 1998.
[34] H. Godrich, A. P. Petropulu, and H. V. Poor, "Power allocation strategies for target localization in distributed multiple-radar architectures," *IEEE Trans. Signal Process.*, vol. 59, no. 7, pp. 3226–3240, Jul. 2011.
[35] A. A. Gorji, R. Tharmarasa, and T. Kirubarajan, "Widely separated MIMO versus multistatic radars for target localization and tracking," *IEEE Trans. Aerosp. Electron. Syst.*, vol. 49, no. 4, pp. 2179–2194, Oct. 2013.
[36] J. Marcum, "A statistical theory of target detection by pulsed radar," *IEEE Trans. Inf. Theory*, vol. IT-6, no. 2, pp. 259–267, Apr. 1960.
[37] Q. He and R. S. Blum, "Noncoherent versus coherent MIMO radar: Performance and simplicity analysis," *Signal Process.*, vol. 92, no. 10, pp. 2454–2463, Oct. 2012.
[38] D. A. Shnidman, "Radar detection probabilities and their calculation," *IEEE Trans. Aerosp. Electron. Syst.*, vol. 31, no. 3, pp. 928–950, Jul. 1995.
[39] Y. Yang, W. Yi, G. Cui, L. Kong, and J. Yang, "Antenna placement for distributed MIMO radar with surveillance performance," in *Proc. IET Int. Radar Conf.*, Hangzhou, China, Oct. 2015, pp. 1–5.
[40] D. A. Shnidman, "The calculation of the probability of detection and the generalized marcum Q-function," *IEEE Trans. Inf. Theory*, vol. 35, no. 2, pp. 389–400, Mar. 1989.
[41] M. E. Liggins, C.-Y. Chong, I. Kadar, M. G. Alford, V. Vannicola, and S. Thomopoulos, "Distributed fusion architectures and algorithms for target tracking," *Proc. IEEE*, vol. 85, no. 1, pp. 95–107, Jan. 1997.
[42] J. Kennedy and R. Eberhart, "Particle swarm optimization," in *Proc. Int. Conf. Neural Netw*, Perth, WA, Australia, Nov. 1995, pp. 1942–1948.
[43] Y. del Valle, G. K. Venayagamoorthy, S. Mohagheghi, J.-C. Hernandez, and R. G. Harley, "Particle swarm optimization: Basic concepts, variants and applications in power systems," *IEEE Trans. Evol. Comput.*, vol. 12, no. 2, pp. 171–195, Apr. 2008.
[44] Y. Yang, T. Zhang, W. Yi, L. Kong, X. Li, B. Wang, and X. Yang, "Deployment of multistatic radar system using multi-objective particle swarm optimisation," *IET Radar, Sonar Navigat.*, vol. 12, no. 5, pp. 485–493, May 2018.
[45] Y. Zou and K. Chakrabarty, "Sensor deployment and target localization based on virtual forces," in *Proc. 22nd Annu. Joint Conf. IEEE Comput. Commun. Societies (INFOCOM)*, San Francisco, CA, USA, Mar./Apr. 2003, pp. 1293–1303.
[46] S. Boyd and L. Vandenberghe, *Convex Optimization*. Cambridge, U.K.: Cambridge Univ. Press, 2004, pp. 658–697.

YAO WANG (Graduate Student Member, IEEE) received the B.E. degree in electrical engineering from the University of Electronic Science and Technology of China (UESTC), China, in 2017, where he is currently pursuing the Ph.D. degree. His current research interests include sensor networks, cognitive resource management, and target detection.

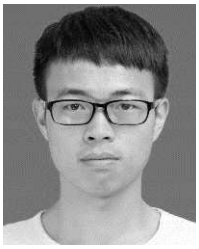

SHIXING YANG (Graduate Student Member, IEEE) received the B.E. degree in electronic information engineering from Harbin Engineering University, Harbin, China, in 2017. He is currently pursuing the Ph.D. degree with the University of Electronic Science and Technology of China (UESTC). His current main research interests include statistical signal processing, radar signal processing, and array signal processing, especially MIMO radar detection technology.

TAO ZHOU (Member, IEEE) received the B.E. degree in electrical engineering from the University of Electronic Science and Technology of China (UESTC), China, in 2015, where he is currently pursuing the Ph.D. degree in signal and information processing. His current main research interests include statistical signal processing, radar signal processing, and array signal processing, especially detection and localization technology.

NA LI (Member, IEEE) received the B.S. degree in electronic engineering from Shandong Normal University, Jinan, China, in 2009, and the Ph.D. degree in signal and information processing from the University of Electronic Science and Technology of China (UESTC), Chengdu, in 2016.

She was with the Department of Electrical Engineering, Duke University, as a Visiting Researcher, from 2013 to 2015. She has been with the School of Information and Communication Engineering, UESTC, as a Research Assistant, since 2018. Her research interests include radar signal analysis and processing.